Journal of Sound and Vibration (1998) **216**(1), 159–185
Article No. sv981708

IMPLEMENTATION AND EXPERIMENTAL VALIDATION OF A NEW VISCOTHERMAL ACOUSTIC FINITE ELEMENT FOR ACOUSTO-ELASTIC PROBLEMS

W. M. Beltman, P. J. M. van der Hoogt, R. M. E. J. Spiering and H. Tijdeman

University of Twente, *Faculty of Mechanical Engineering*, *P.O. Box* 217, 7500 *AE Enschede*, *The Netherlands*

(*Received* 18 *June* 1997, *and in final form* 23 *April* 1998)

The propagation of sound waves in thin gas or fluid layers can be significantly affected by viscothermal phenomena. In this paper, a new viscothermal acoustic finite element is presented. The element includes the effects on inertia, viscosity, compressibility and thermal conductivity. The acoustic element can be coupled to flexible structural elements. This enables fully coupled acousto-elastic calculations to be made for complex geometries. The model is experimentally validated with measurements on a rigid airtight box with a flexible coverplate. Eigenfrequencies, damping and mode shapes of the plate were measured and compared with numerical results for a number of gas layer thicknesses. The agreement between measurements and calculations is good. The results indicate that there can be large shifts in eigenfrequency as a function of the layer thickness. In addition, for small layer thicknesses a high damping value is found, which can be attributed to viscous effects in the layer.

1. INTRODUCTION

This paper deals with a numerical and experimental study on the interaction between a thin layer of gas (in most cases air) and a vibrating structure. Because the air layer is thin, effects of viscosity and thermal conductivity can play an important role. Furthermore, the acousto-elastic coupling can be very strong for this situation. To the authors' knowledge, no general method is available for calculations.

In a previous paper a model was presented which describes the propagation of sound waves in a thin layer [1]. However, the model for the air layer was applied only to rigid surfaces. Results from analytical calculations and experiments were compared for an oscillating, rigid solar panel. In the present paper the model is extended to flexible surfaces, including the acousto-elastic interaction. For this purpose, a new viscothermal acoustic finite element is presented which is based on the thin layer model. This element can be coupled with structural finite elements, enabling fully coupled calculations for complex geometries.

Due to its multidisciplinary character, this type of problem inspired researchers from various fields. In tribology, the main interest was the calculation of squeeze film damping between rotating or oscillating machine parts [2–6]. Several authors focused on the importance of the inertial terms in the layer model. They showed that one has to pay

0022–460X/98/360159 + 27 $30.00/0

serious attention to the assumptions on which the Reynolds equation is based. For high values of a modified Reynolds number, the inertial effects have to be taken into account. For these situations, for instance at high speeds or frequencies, the so-called creeping flow assumption of the Reynolds equation breaks down.

In the field of fluid mechanics a number of models were presented; see, e.g., reference [7]. In most cases the research was aimed at the calculation of the so-called steady streaming. Consider for instance a rigid plate, located parallel to a fixed surface and performing an oscillation normal to the surface. In a linearized model, the force acting on the plate due to the pressure distribution is purely oscillatory with a frequency corresponding to the driving frequency. When the second order terms are taken into account, a steady force acting on the plate is obtained. This force, caused by the steady streaming, has been described in several papers [8, 9]

In acoustics the higher order terms are usually neglected. The first papers on thin film theory in the field of acoustics were presented by Maidanik [10] and Ungar and Carbonell [11]. Since then a number of models were developed; see e.g., the book by Pierce [12]. Most of them incorporate the effects of viscosity, inertia and thermal conductivity in the air layer. Some also incorporate compressibility and bulk viscosity. Key words in the characterization of the different models are: pressure gradient across layer thickness, acousto-elastic coupling and ability to model complex geometries. Based on these key words, the layer models in acoustics can be divided into three groups.

The first group concerns models which assume a constant pressure across the layer thickness. This leads to a straightforward, yet practical very useful, description. This approach was successfully described and used by Fox and Whitton [13], Önsay [14, 15]. They used a fully coupled approach to determine the interaction between a vibrating plate a thin layer of air. However, the practical use of their models is limited to simple geometries like strips.

The second group incorporates a pressure gradient across the layer thickness. Some extra terms of the Navier Stokes equations are taken into account for this purpose. However, in most cases the acousto-elastic coupling is not accounted for. In the paper of Trochidis [16], the free vibration modes of infinite plates are imposed as boundary conditions for the layer model. The resulting pressure distribution was used to calculate the loss factor of the system. This lack of coupling results in a serious limitation of the model, as will be shown later in the present paper. Möser [17] extended the Trochidis model with compressibility effects. He calculated the eigenfrequencies and damping values of a coupled plate–layer system. His analysis was limited to infinite plates where the displacement is a function of one co-ordinate only. Chow and Pinnington [18, 19] investigated practical methods for the squeeze film damping mechanism with air and liquids. In their analysis they used an impedance formulation for the layer, which was based on an extended version of the Trochidis model.

The third group concerns the most extensive model for the air layer. It is based on a solution of the full set of linearized basic equations, e.g., the Navier Stokes equations, including the bulk viscosity of the air. Actually this results in an extended version of the equation developed by Kirchhoff, which was also described by Rayleigh [20]. In comparison to the other models this leads to a very complicated model, as described in papers by Bruneau *et al*. [21, 22], and Plantier and Bruneau [23]. This type of model was developed to calculate the interaction between a vibrating membrane and a rigid backing electrode in miniaturized transducers. The membrane and the backing electrode are separated by a thin layer of air. For these applications the frequency range is very wide, e.g., up to 20 kHz. Therefore, it was argued that one had to include all the terms in the Navier Stokes equations.

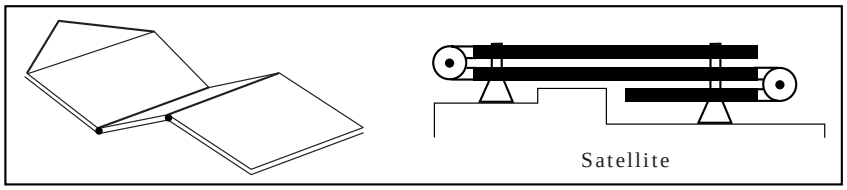

Figure 1. Solar array in deployment and in folded position

The interaction between the air layer and the membrane is usually accounted for. Recently, Karra, *et al*. [24] presented a numerical formulation for this model. Their formulation, however, is limited to geometries with rotatory symmetry.

The new finite element presented in this paper is based on the model with a constant pressure across the layer thickness (first group). However, because the formulation is written in terms of dimensionless parameters, one can determine the validity of the model in a very easy way. Furthermore, the finite element model can be used to model complex geometries and it includes the full acousto-elastic coupling.

The finite element model can be used to analyze, for instance, the damping capabilities of double wall panels. It offers an efficient tool for the designer when optimizing the damping due to the squeeze film mechanism in the layer. It can also be used to calculate the interaction between a vibrating membrane and the rigid backing electrode in miniaturized transducers. In a preliminary phase the model was applied to analyze the pressure distribution between solar panels in an array (see Figure 1) [25].

During launch the panels are folded against the body of the satellite, thus entrapping a thin layer of air. The solar panels are relatively large and light. The layer of air now has a substantial influence on the dynamical behaviour of the system. With the new finite element model the wave propagation in the layer can be described accurately. It also includes the acousto-elastic interaction, which is essential for a good description of the behaviour of the system.

2. FORMULATION OF THE PROBLEM

A flexible plate is located parallel to a fixed surface (see Figure 2). The plate has dimensions $2l_x \times 2l_y$. A layer of air with mean thickness h_0 is trapped between the plate and the fixed surface. The ends of the layer can be open or closed.

Dimensionless co-ordinates are introduced according to

$$x = \bar{x}/l_x, \qquad y = \bar{y}/l_y, \qquad z = \bar{z}/h_0. \tag{1}$$

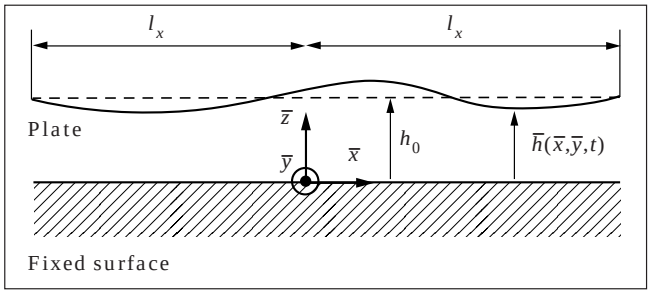

Figure 2. Flexible plate and thin air layer.

The distance between the plate and the fixed surface can be written as the real part of

$$\bar{h}(x, y, t) = h_0[1 + h(x, y)\, e^{i\omega t}], \tag{2}$$

where ω denotes the angular frequency, t represents time, h_0 is the mean gap width, $h(x, y)$ is the dimensionless amplitude of oscillation of the plate and i is the imaginary unit. The plate performs a small harmonic oscillation with frequency ω and amplitude $h_0\, h(x, y)$ around the equilibrium position h_0. (A list of symbols is given in Appendix D.)

3. BASIC THEORY

In this section, the basic equations governing the motion of the plate and the pressure distribution in the air layer are derived. These equations are all written in a dimensionless form. The resulting dimensionless parameters can be used to identify, for instance, different flow regimes in the air layer. Furthermore, the parameters are a useful tool in expressing the range of validity.

3.1. NARROW GAP MODEL

The pressure distribution in the air layer is governed by the following basic equations: the Navier Stokes equations, the equation of continuity, the equation of state for an ideal gas and the energy equation. In the absence of mean flow, dimensionless quantities are introduced [1]:

$$\begin{aligned} \bar{u} &= c_0 u(x, y, z)\, e^{i\omega t}, & \bar{p} &= p_0[1 + p(x, y, z)\, e^{i\omega t}], \\ \bar{v} &= c_0 v(x, y, z)\, e^{i\omega t}, & \bar{\rho} &= \rho_0[1 + \rho(x, y, z)\, e^{i\omega t}], \\ \bar{w} &= c_0 w(x, y, z)\, e^{i\omega t}, & \bar{T} &= T_0[1 + T(x, y, z)\, e^{i\omega t}]. \end{aligned} \tag{3}$$

Here u, v and w are the dimensionless amplitudes of the velocities in the x, y and z directions, respectively.

The dimensionless amplitudes of the perturbations in pressure, density and temperature are denoted by p, ρ and T, respectively. The mean conditions are characterized by an undisturbed speed of sound c_0, a pressure p_0, a density ρ_0 and a temperature T_0. These definitions are used to rewrite the basic equations in a linearized, non-dimensional form. As a result the following dimensionless parameters appear in these equations:

$$\begin{aligned} s &= h_0\sqrt{\rho_0\omega/\mu}, \text{ shear wave number}, & \gamma &= C_p/C_v, \text{ ratio of specific heats}, \\ \sigma &= \sqrt{\mu C_p/\lambda}, \text{ root of Prandtl number}, & g &= h_0/l_x, \text{ narrowness of the gap}, \\ k &= \omega h_0/c_0, \text{ reduced frequency}, & a &= l_y/l_x, \text{ aspect ratio of the panel}. \end{aligned} \tag{4}$$

Here μ is the viscosity, λ is the thermal conductivity, C_p is the specific heat at constant pressure and C_v is the specific heat at constant volume.

The shear wave number is a measure for the ratio between the inertial forces and viscous forces. For low shear wave numbers the viscous effects dominate, whereas for high shear wave numbers the inertial effects dominate. In physical terms it represents the ratio between the gap width and the boundary layer thickness. The reduced frequency is a measure for the ratio between the gap width and the acoustic wavelength.

Next, the walls are assumed isothermal and a no-slip condition is imposed on the upper and lower surfaces. When the in-plane velocities are large in comparison with the velocity in the z direction and the gap width is small in comparison with the acoustic wavelength (one can verify that the conditions $k \ll 1$ and $k/s \ll 1$ have to hold), the set of basic equations

can be rewritten to one equation in terms of the pressure perturbation (see Appendix A) [1, 25, 26]:

$$\frac{\partial^2 p}{\partial x^2} + \left[\frac{1}{a}\right]^2 \frac{\partial^2 p}{\partial y^2} + \frac{k^2\gamma}{g^2 n(s\sigma)B(s)}\, p = -\frac{k^2\gamma}{g^2 B(s)}\, h. \tag{5}$$

Here

$$B(s) = 2\left[\frac{1-\cosh(s\sqrt{\mathrm{i}})}{s\sqrt{\mathrm{i}}\sinh(s\sqrt{\mathrm{i}})}\right] + 1, \qquad n(s\sigma) = \left[1 - \left[\frac{\gamma-1}{\gamma}\right] B(s\sigma)\right]^{-1}. \tag{6}$$

Note that, due to the assumptions, the pressure is constant across the gap width. This explains the fact that equation (5) does not contain partial derivatives with respect to z. The function $B(s)$ accounts for the viscous effects in the air layer. For large values of the shear wave number this function reduces to 1; for low shear wave numbers it can be written as $\mathrm{i}s^2/12$.

The function $n(s\sigma)$ solely accounts for the thermal effects in the layer, since the quantity $s\sigma$ does not depend on the viscosity μ. It can be interpreted as a polytropic constant that relates density and pressure according to a polytropic law. For low values of $s\sigma$ the quantity n reduces to 1, corresponding to isothermal conditions. For high values of $s\sigma$ it reduces to γ, corresponding to adiabatic conditions. The value of σ is constant for a given medium, e.g., air. These considerations imply that for low shear wave numbers the narrow gap equations reduces to a linearized version of the Reynolds equation. For high shear wave numbers a modified version of the wave equation is obtained. The modification is due to the fact that the pressure is assumed constant across the layer.

The dimensionless equation for general values of s can be rewritten in a dimensional form as

$$\frac{\partial^2 \bar{p}}{\partial \bar{x}^2} + \frac{\partial^2 \bar{p}}{\partial \bar{y}^2} + \frac{\omega^2}{c_{eff}(s)^2}\, \bar{p} = -\frac{\rho_0 \omega^2}{B(s)}\, h, \tag{7}$$

where

$$c_{eff}(s) = c_0 \sqrt{\frac{n(s\sigma)}{\gamma}\, B(s)}. \tag{8}$$

Equation (7) resembles the classical wave equation. A source term is present on the right-hand side due to the squeeze motion of the plate. The quantity $c_{eff}(s)$ can be interpreted as an effective speed of sound. Its value is affected by viscous effects, accounted for in $B(s)$, and thermal effects accounted for in $n(s\sigma)$. Notice that the effective speed of sound is shear wave number, e.g., frequency, dependent. For high values it reduces to the undisturbed speed of sound c_0.

3.2. PLATE MODEL

The Kirchhoff equation is used to describe the deformation of the plate. In a non-dimensional form this equation is

$$\frac{\partial^4 h}{\partial x^4} + 2\left[\frac{1}{a}\right]^2 \frac{\partial^4 h}{\partial x^2\, \partial y^2} + \left[\frac{1}{a}\right]^4 \frac{\partial^4 h}{\partial y^4} - \Omega^2 h = \frac{\Omega^2 \varepsilon}{k^2 \gamma}\, p, \tag{9}$$

where the following two dimensionless parameters are introduced:

$$\Omega = \omega\sqrt{l_x^4 \rho_p t_p / D_p}, \quad \text{dimensionless frequency}$$

$$\varepsilon = \rho_0 h_0 / \rho_p t_p, \quad \text{ratio of mass per unit area between plate and air layer.} \tag{10}$$

Here t_p and ρ_p are the thickness and the density of the plate. D_p represents the bending stiffness of the plate according to

$$D_p = E_p t_p^3 / 12(1 - v_p^2), \tag{11}$$

where E_p and v_p are Young's modulus and Poisson's ratio of the plate material. The parameter ε is a coupling parameter. It indicates that the ratio between the mass per unit area of the plate and the medium is a factor which affects the amount of coupling.

3.3. ACOUSTO-ELASTIC MODEL

The acousto-elastic interaction is established by demanding continuity of velocity across the interface. One therefore has to solve the narrow gap equation (5) and the plate equation (9) simultaneously. Generally speaking, it is possible to solve these equations analytically only for simple geometries and simple boundary conditions. In order to be able to model more realistic situations, a new finite element model will be presented in the next section.

4. FINITE ELEMENT FORMULATION

4.1. ACOUSTIC MODEL

The basic equation for the new acoustic finite element is the narrow gap equation. In dimensional form, this equation is

$$\frac{\partial^2 \bar{p}}{\partial \bar{x}^2} + \frac{\partial^2 \bar{p}}{\partial \bar{y}^2} + \frac{\omega^2}{c_{eff}(s)^2} \bar{p} = -\frac{\rho_0 \omega^2}{B(s)} h. \tag{12}$$

The equation resembles the standard wave equation. Therefore, in an entirely similar way a finite element formulation can be derived. The only differences with standard acoustic elements are the following.

It is a 2-dimensional element because equation (12) was obtained by integration across the layer thickness. Only in-plane pressure gradients exist.

An excitation term is present due to the squeeze motion of the surfaces. The differential equation (12) was obtained by integration, resulting in the source term due to the squeeze motion.

The undisturbed speed of sound, c_0, is replaced by the effective speed of sound, $c_{eff}(s)$.

If one takes into account these considerations this leads to the following set of equations (see Appendix B):

$$-\omega^2[M^a(s)]\{\mathbf{P}\} + [K^a]\{\mathbf{P}\} = \omega^2[M^c(s)]\{\mathbf{U}\}. \tag{13}$$

Here $[M^a(s)]$ denotes the acoustic mass matrix, $[K^a]$ is the acoustic stiffness matrix, $\{\mathbf{P}\}$ is the vector of the nodal pressure degrees of freedom, $\{U\}$ is the vector of the nodal structural degrees of freedom and $[M^c(s)]$ is the coupling matrix.

Because the effective speed of sound is complex and depends on the shear wave number, the acoustic mass matrix is also complex and shear wave number, e.g., frequency, dependent. In fact, the mass matrix is equal to the corresponding standard acoustic mass matrix, but it is premultiplied by $1/c_{eff}(s)^2$ instead of $1/c_0^2$. A linear 4-noded (Q4.VISC) and a quadratic 8-noded element (Q8.VISC) were implemented in the finite element package B2000 [27]. This is a transparent finite element package in which one's own developments

and elements can be implemented in an easy way. The viscothermal elements are equipped with a number of key options which can be used to activate or deactivate for instance viscosity or thermal conductivity. The elements can thus degenerate to modified wave equation elements or elements for the linearized Reynolds equation. The elements will be validated by comparing the results with analytical results in section 4.5 for an oscillating rigid panel.

4.2. STRUCTURAL MODEL

The finite element model for the structure, in the absence of structural damping, can be written in the following standard formulation (see Appendix B):

$$-\omega^2[M^s]\{\mathbf{U}\} + [K^s]\{\mathbf{U}\} = [K^c]\{\mathbf{P}\} + \{\mathbf{F}^{ext}\}. \tag{14}$$

Here $[M^s]$ denotes the structural mass matrix, $[K^s]$ is the stiffness matrix, $\{\mathbf{U}\}$ is the vector with the nodal degrees of freedom, $[K^c]$ is the coupling matrix resulting from the pressure on the interface and $\{\mathbf{F}^{ext}\}$ is the external nodal force vector.

4.3. ACOUSTO-ELASTIC MODEL

The acousto-elastic interaction is established by demanding continuity of normal velocity across the interface. This leads to the following coupled system of equations (see Appendix B):

$$-\omega^2\begin{bmatrix}[M^s] & [0]\\ [M(s)^a] & [M^a(s)]\end{bmatrix}\begin{Bmatrix}\{\mathbf{U}\}\\ \{\mathbf{P}\}\end{Bmatrix} + \begin{bmatrix}[K^s] & -[K^c]\\ [0] & [K^a]\end{bmatrix}\begin{Bmatrix}\{\mathbf{U}\}\\ \{\mathbf{P}\}\end{Bmatrix} = \begin{Bmatrix}\{\mathbf{F}^{ext}\}\\ \{\mathbf{0}\}\end{Bmatrix}. \tag{15}$$

This system contains the mass matrices and the stiffness matrices of the structural part and the acoustic part. The coupling is established by the two coupling matrices, $[M^c(s)]$ and $[K^c]$, which are related by

$$[M(s)^c] = (\rho_0/h_0 B(s))\,[K^c]^{\mathrm{T}}. \tag{16}$$

The coupling matric $[K^c]$ is equal to the standard acoustic coupling matrix for this situation. The matrix $[M^c(s)]$ differs from the standard coupling matrix only due to the premultiplication factor given in equation (16).

4.4. SOLUTION PROCEDURE

The system of equations (15) is complex and asymmetric. Furthermore some of the matrices involved are shear wave number, e.g., frequency, dependent. Because an eigenvalue solver for complex, asymmetric and frequency dependent matrices was not available yet, an iterative approach was adopted [28]. The iterative process starts with a first estimate of the expected eigenfrequency. The acoustic matrices are calculated and the coupled system is assembled. For this system of equations, the eigenfrequencies are calculated. A solver for complex, asymmetric eigenvalue problems is used in this step. The eigenfrequency closest to the expected frequency (in an absolute sense since they are complex numbers) is then used to construct the matrices for the second iteration step. This process is repeated until the frequency has converged. Convergence is obtained if the frequency value that was used to construct the acoustic matrices is within a specified tolerance of the resulting calculated eigenfrequency.

In order for the process to converge, a good first estimate is required. In the present paper the acousto-elastic coupling is investigated by varying the gap width (see sections 5 and 6). The first calculation was carried out for a large gap width. For this gap width the damping is very low and the eigenfrequencies can be estimated by simple wave equation

and plate models. Successive calculations were carried out for decreasing gap widths. The values that were already obtained for a large gap width were used to estimate the eigenfrequency. In this way a good first estimate of the complex eigenfrequency could be provided.

4.5. ANALYTICAL VALIDATION OF THE VISCOTHERMAL ACOUSTIC FINITE ELEMENT

Consider a rigid plate, located parallel to a fixed surface and performing a small normal oscillation. For this situation the displacement amplitudes for all the points on the panel are equal: $h(x, y) = h$. When the end of the layer are open, i.e., a $p = 0$ condition is imposed for $x = \pm 1$ and $y = \pm 1$, one obtains the following pressure distribution (see, e.g., reference [1]):

$$p(x, y) = \frac{4k^2\gamma h a^2}{\pi g^3 B(s)} \sum_{q=1,3,..} \frac{(-1)^{q-1/2}}{qD^2} \left[1 - \frac{\cosh(Dy)}{\cosh(D)}\right] \cos\left[\frac{q\pi}{2} x\right]. \tag{17}$$

Here:

$$D = \sqrt{\left[\frac{q\pi}{2} a\right]^2 - \frac{k^2 a^2 \gamma}{g^2 n(s\sigma) B(s)}}. \tag{18}$$

The pressure distribution was also calculated with linear 4-noded and quadratic 8-noded viscothermal finite elements. The number of elements was varied in order to investigate if the numerical results converge to the analytical values. The properties of the air in the gap under standard atmospheric conditions, the dimensions of the plate, the thickness of the air layer and the frequency of interest are as follows:

$$\mu = 18{\cdot}2 \times 10^{-6}\ \text{Ns/m}^2, \quad \lambda = 25{\cdot}6 \times 10^{-3}\ \text{W/mK}, \quad \rho_0 = 1{\cdot}2\ \text{kg/m}^3, \quad T_0 = 293\ \text{K},$$
$$c_0 = 340\ \text{m/s}, \quad C_p = 1004\ \text{J/kgK}, \quad C_v = 716\ \text{J/kgK},$$
$$l_x = 0{\cdot}5\ \text{m}, \quad l_y = 0{\cdot}5\ \text{m}, \quad h_0 = 1\ \text{mm}, \quad f = 50\ \text{Hz}. \tag{19}$$

The shear wave number for this problem is 4·5. Therefore, both the effects of inertia and viscosity are important. The value of the reduced frequency is approximately 10^{-3}: the wave length is large compared to the layer thickness. It can be concluded that these conditions are suited for a proper test of the new viscothermal finite element.

In Table 1 the results are listed. In this table *nex* and *ney* represent the number of elements in the x and the y directions, respectively. For each calculation, the maximum difference between the numerical and analytical results in the center node, divided by the maximum absolute value of the pressure from the analytical expression is given. The results indicate that the numerical results converge to the analytical values. It can be concluded that the viscothermal finite element gives good results.

TABLE 1

Maximum relative error for Q4.VISC *and* Q8.VISC *elements*

nex	*ney*	Q4.VISC	Q8.VISC
4	4	0·051270	0·0100847
8	8	0·011867	0·0002707
16	16	0·002948	0·0000138

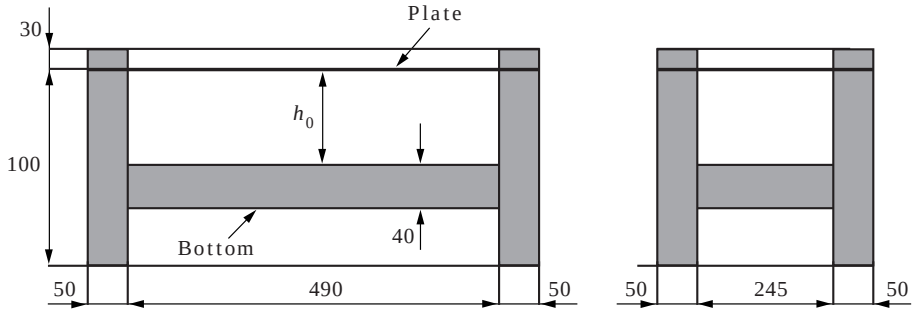

Figure 3. Airtight box with flexible coverplate; dimensions in mm.

5. EXPERIMENTS

5.1. EXPERIMENTAL SET-UP

To validate the viscothermal model including acousto-elastic interaction, experiments were carried out on an airtight box with a flexible coverplate (see Figure 3). This experiment was described in a paper by Dowell *et al*. [29]. Their analysis, however, was limited to large gap widths and did not include viscothermal effects. The set-up is very simple, yet very useful, to illustrate the different mechanisms at work.

The plate is an aluminium plate, $0{\cdot}49 \times 0{\cdot}245$ m, with a thickness of 1 mm. The plate is clamped at the edges. The box itself is also made of aluminium to avoid unwanted effects due to differences in thermal expansion of the materials. The walls of the box are 50 mm thick. The gap width, h_0, can be varied between 1 and 50 mm by displacement of the bottom. The material and geometrical properties of the aluminium plate are

$$E_p = 70 \times 10^9 \text{ N/m}^2, \qquad \rho_p = 2710 \text{ kg/m}^3, \qquad v_p = 0{\cdot}3, \qquad t_p = 1 \times 10^{-3} \text{ m}. \quad (20)$$

The properties of the air in the gap under standard atmospheric conditions were given in equation (19). The plate is excited by an electrodynamic shaker (Brüel & Kjær 4810) with a random signal in the frequency range up to 512 Hz (see Figure 4). The point of excitation was chosen in such a way that it did not coincide with a node of one of the eigenmodes in this frequency range. The input force was measured with a force transducer (Brüel & Kjær 8203). One accelerometer was mounted on the bottom and a number of accelerometers (Brüel & Kjær 4374) were mounted on the plate to measure the response of the system. All signals were amplified (Brüel & Kjær 2626 and 2650) and fed to a front end (HP 3565). The data was transferred to a workstation where a modal analysis was conducted: eigenfrequencies, damping and the mode shapes were determined for a number of gap widths (LMS CADA-X package).

5.2. ACCURACY OF THE EXPERIMENTS

5.2.1. *Eigenfrequencies in absence of the bottom*

As a first check of the model, the eigenfrequencies of the plate in the absence of the bottom were measured. In this case one measures the eigenfrequencies of a clamped rectangular plate in an infinite air domain. The structural modes, i.e., the modes of the plate in vacuum, can be calculated analytically. In order to account for the influence of the surrounding air, an added mass was calculated according to the formula given by Blevins [39]. This small amount of added mass causes a small decrease in eigenfrequency. The calculated (in air and vacuum) and measured frequencies are listed in Table 2. In this table "qr" represents the number of half wave lengths in the x and the y directions,

TABLE 2

Eigenfrequencies of clamped plate in infinite air domain

Mode qr	Eigenfrequency (Hz)		
	Measurements	Analytical (air)	Analytical (vacuum)
11	9·62	95·9	100·6
21	130·1	130·4	130·4
31	181·8	182·6	183·4
12	247·4	261·7	261·7
41	253·8	259·7	259·7
22	280·8	291·2	291·2
32	322·6	341·0	341·0

respectively. There is fair agreement between the calculations and the experiments. A further discussion on the structural modes will be presented in section 6.1.

5.2.2. *Damping in the absence of bottom plate*

The damping of the plate in the absence of the bottom plate was measured and found to be in the order of magnitude of 0·7% for the first seven modes. This damping is relatively high and is mainly caused by the damping due to the clamping of the thin plate. In order to support this statement, the amount of radiation damping was estimated with the boundary element package SYSNOISE [31]. In the calculations, the structural mesh consisted of 20 × 20 shell elements. The first eigenfrequency of the plate in vacuum for this mesh was 100·9 Hz. For an estimation of the radiation damping, a frequency response calculation was carried out. The structural mesh was coupled to a mesh of 20 × 20 boundary elements. An indirect variational approach was used. The plate was excited by a point force and the resulting displacements were calculated. Eigenfrequency and damping

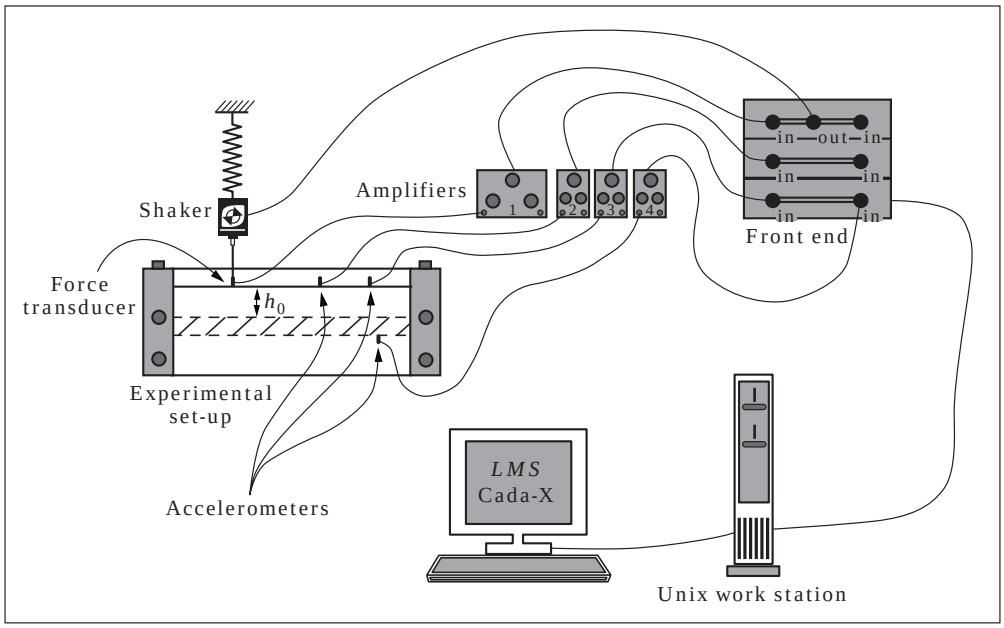

Figure 4. Schematic view of the experimental set-up.

were extracted from the frequency response results. The eigenfrequency in an infinite air domain was found to be 97·4 Hz, while the amount of radiation damping was less than 0·1%. This supports the assumption that the damping due to acoustic radiation can be neglected compared to the other damping mechanisms.

5.2.3. *Boundary conditions*

Careful attention has to be paid to the clamping conditions of the plate. The experimental results in section 5.2.1 showed fair agreement with the calculations. In the experiments the bolts were fastened with the torque of 60 Nm. In order to determine the influence of the torque, measurements were carried out for variations in this torque. No variations in frequencies were observed due to a change in applied torque.

5.2.4. *Linearity*

In the experiments the plate is excited with a constant force. In order to check if the system behaves linearly, experiments were carried out with different excitation levels. The eigenfrequencies and the damping values were not affected by the amplitude of excitation. This justifies the use of linear theory.

5.2.5. *Motion of the bottom plate*

In the calculations it is assumed that the box and the bottom plate are rigid and fixed. Since the gap width is a very important parameter in the model, the motion of the bottom plate was measured with accelerometers for a number of gap widths. In all cases the amplitude of the bottom plate was very low, i.e., less than 3%, compared to the amplitude of the flexible coverplate. The bottom plate can therefore be regarded as rigid and fixed.

5.2.6. *Variation of the gap width*

In the experiments the gap width is varied from 1 to 50 mm. Due to the fact that the thick bottom plate is not able to tilt inside the box, the variation in the gap width is small. This variation is estimated to be $\pm 0{\cdot}1$ mm.

6. RESULTS FOR THE EXPERIMENTAL SET-UP

In this section the results for the airtight box with the flexible coverplate are presented. As a check on the accuracy of the finite element model for the experimental set-up, the uncoupled modes for the plate and the air layer are calculated and compared to analytical solutions in sections 6.1 and 6.2, respectively. An additional reason for calculating the uncoupled modes is that one has a reference, from which the importance of coupling can be demonstrated. Finally, in section 6.3 the finite element results for the acousto-elastic system are compared with experimental results.

6.1. STRUCTURAL MODES

The eigenfrequencies of the plate in vacuum were calculated with a mesh of 20×20 linear plate elements and compared with analytical results [29]. The results are listed in Table 3. The table shows fair agreement between the numerical results and the analytical results. For the higher modes the results start to be less accurate due to the small number of elements. The first seven mode shapes for the plate in vacuum are given in Figure 5 because they serve as a reference when the mode shapes change as a function of the gap width.

TABLE 3

Eigenfrequencies of clamped plate in vacuum

Mode qr	Eigenfrequency (Hz)	
	Analytical (vacuum)	Finite elements
11	100·6	100·9
21	130·4	131·1
31	183·4	186·9
12	261·7	266·1
41	259·7	270·8
22	291·2	295·2
32	341·0	346·8

6.2. ACOUSTIC MODES

The acoustic modes are the modes of the air layer when the plate is assumed rigid and fixed (zero velocity). The acoustic modes can therefore be obtained from the narrow gap equation (see section 3.2) by omitting the squeeze term:

$$\frac{\partial^2 \bar{p}}{\partial \bar{x}^2} + \frac{\partial^2 \bar{p}}{\partial \bar{y}^2} + \frac{\omega^2}{c_{eff}(s)^2}\bar{p} = 0. \tag{21}$$

The edges of the air layer are closed. The corresponding boundary condition is that the particle velocity is zero. The narrow gap model gives the following boundary condition in terms of the pressure:

$$\frac{\partial \bar{p}}{\partial \bar{n}} = 0 \quad \text{for } \bar{x} = \pm l_x \quad \text{and} \quad \bar{y} = \pm l_y. \tag{22}$$

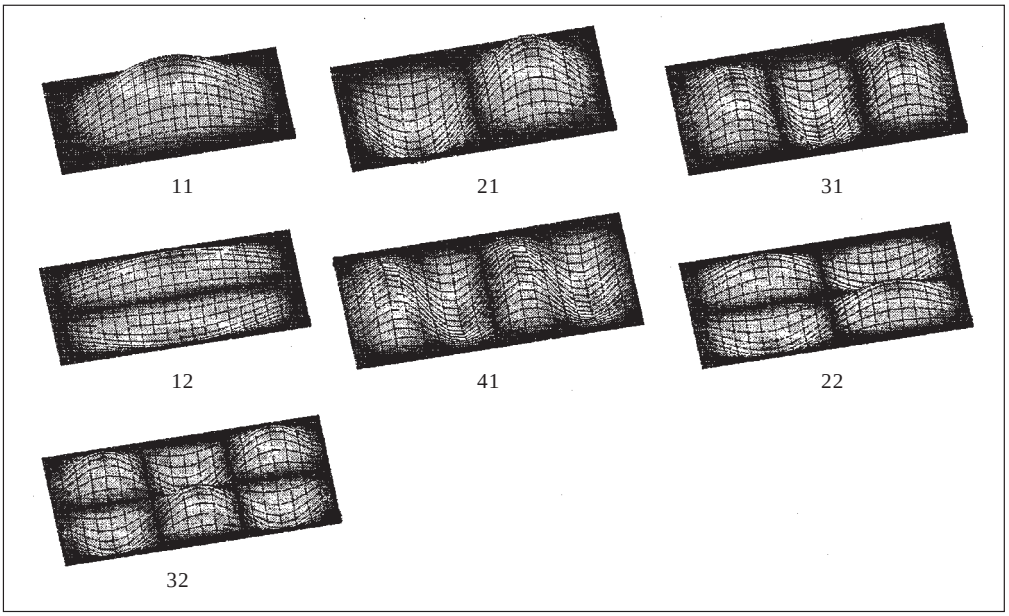

Figure 5. Mode shapes in vacuum.

TABLE 4

Eigenfrequencies of air layer ($h_0 = 1$ *mm*)

		Eigenfrequency (Hz)	
Mode	qr	Analytical	Finite elements
1	10	317·1 + 32·3 i	317·4 + 32·4 i
2	01	651·4 + 44·8 i	652·1 + 44·8 i
3	20	651·4 + 44·8 i	654·1 + 45·0 i
4	11	730·9 + 47·2 i	731·6 + 47·3 i

Here $\bar{n}$ is the outward normal. Straightforward separation of variables gives an equation for the acoustic eigenfrequencies:

$$\omega = \frac{\pi c_{eff}(s)}{2} \sqrt{\left[\frac{q}{l_x}\right]^2 + \left[\frac{r}{l_y}\right]^2}, \quad q = 0, 1, 2, \ldots, \quad r = 0, 1, 2, \ldots. \tag{23}$$

Since the effective speed of sound is a function of the shear wave number, the right-hand side of equation (23) depends on the frequency and the gap width. The complex eigenfrequencies can now be obtained from this equation by a simple iterative solving procedure. As starting values, the eigenfrequencies for the inviscid, adiabatic case are used: $c_{eff}(s) = c_0$. In Table 4, the analytical results and the results from finite element calculations are listed for a gap width of 1 mm. The calculations were carried out with 20 × 20 linear viscous acoustic finite elements. The table shows good agreement between the analytical results and the finite element results. The first acoustic mode without viscous or thermal effects is 347 Hz. For low shear wave numbers the viscous and thermal effects therefore have a strong influence on the propagation of waves in the air layer.

6.3. ACOUSTO-ELASTIC MODES: COMPARISON WITH EXPERIMENTAL RESULTS

In the case of a thin plate backed by a cavity with air, the acousto-elastic coupling can be very strong. In this section this phenomenon will be demonstrated. For this purpose the first seven eigenfrequencies of the plate will be calculated as a function of the gap width. The eigenfrequency, damping and mode shapes are traced in the calculations for gap widths from 300 down to 1 mm. For gaps below 50 mm a comparison is made with the experimental results.

The mode shapes and the eigenfrequencies for a gap width of 300 mm are very close to the mode shapes and the eigenfrequencies in vacuum. When the gap width is decreased, eigenfrequencies and mode shapes are strongly affected. By tracing the modes from 300 down to 1 mm, the complete evolution of the different modes can be visualized.

The choice of the first seven modes is based on the fact that these modes remain isolated. This means that these modes may show a shift in frequency or even mutual cross-overs, but they remain isolate from the higher (i.e., eighth and higher) modes. Note that the first acoustic eigenfrequency in the absence of viscous or thermal effects is 347 Hz. Due to the viscous effects this frequency will decrease (see section 6.2). The first seven modes of interest, however, are all structurally dominated modes.

In order to trace the modes from 300 down to 1 mm two types of calculations were carried out.

The first type of calculation uses standard acoustic finite elements without viscous or thermal effects. These elements were used for the calculations for gap widths between 50

and 300 mm. For these gap widths the shear wave number is very large in the frequency range of interest, so viscous and thermal effects can be neglected. Furthermore, the assumption of constant pressure across the gap width breaks down for large reduced frequencies. Note that the damping for these elements is always zero. A mesh consisting of 20 × 20 plate elements, 20 × 20 linear interface elements and 20 × 20 × 6 acoustic finite elements was used.

The second type of calculation is based on the use of viscous acoustic finite elements. These elements are used for gap widths below 50 mm. A mesh consisting of 20 × 20 linear plate elements, 20 × 20 linear interface elements and 20 × 20 linear viscous acoustic finite elements was used to perform these calculations.

The influence of the air on the upper side of the plate is not taken into account in the calculations. In section 5.2.1 it was demonstrated that the air on the upper side of the panel causes a slight decrease in eigenfrequency. For low gap widths, however, this effect can be neglected compared to the shift in frequency due to the air in the layer. The air on the upper side introduces an energy loss due to radiation damping. However, in section 5.2.2 it was shown that the radiation damping can be neglected compared to the other damping mechanisms (see also section 6.3.2).

6.3.1. *Eigenfrequency*

In Figure 6 the eigenfrequency is depicted versus the gap width. The labels for the different modes are based on the original modes in vacuum (see Table 2). The experimental results and the finite element results show fair agreement. For the lower modes the results are very good. For the higer modes the finite element results start to be less accurate due to the amount of elements. This can mainly be attributed to the behaviour of the plate elements, as can be seen in the results for the structural modes. But on the whole the agreement is satisfying for all modes under consideration.

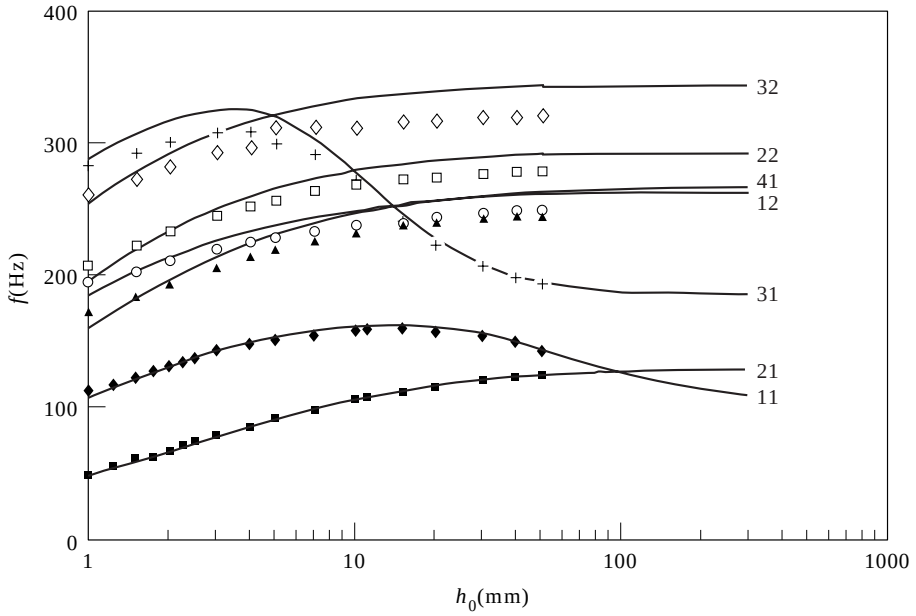

Figure 6. Calculated and measured eigenfrequencies. Experimental: ◇, 32; □, 22; ○, 41; ▲, 12; +, 31; ■, 21; ◆, 11.

At a gap width of 50 mm the transition from the results with standard acoustic elements to the results with viscous finite elements is very good. There seems to be a slight bend in the curve, but the difference in frequency between both calculations is less than 0·7% for this gap width.

The figure shows a very large shift in eigenfrequency for the different modes. The coupled eigenfrequencies differ a great deal from the uncoupled structural eigenfrequencies. This shows that in the case of narrow gaps it is essential to take into account the acousto-elastic coupling.

Different kinds of behaviour can be observed in this figure. The second mode for instance shows a steady decrease with decreasing gap width. The first mode however first increases and then decreases with decreasing gap width. At a gap width of about 100 mm the eigenfrequencies cross. In order to analyze this in more detail, several calculations were carried out in this region. The results clearly indicate that indeed there is a cross-over. The 31-mode also exhibits cross-over behaviour with other modes. Note that cross-overs only occur between symmetric and asymmetric modes. There are two symmetric modes, the 12-mode and the 41-mode, that are very close in frequency. As the gap width decreases, the two frequency values approach. However, when the gap width is further decreased, the difference increases. In Appendix C a simple representative mechanical system is presented which illustrates that cross-overs are not unusual for this type of system.

6.3.2. *Damping*

In Figure 7 the dimensionless damping coefficient is depicted versus the gap width for the first and the second mode. For small gaps the damping increases up to 25%. This high level of damping can be attributed to the viscous effects in the air layer. The damping is high for the second mode. This is an asymmetric mode that induces a strong pumping of air in the layer. The corresponding high rate of shear results in significant viscous losses. Thermal effects have a very small influence on the damping, as was already demonstrated by Fox and Whitton [13]. The damping due to acoustic radiation is low compared to the other damping mechanisms for small gap widths. The figure shows fair agreement between

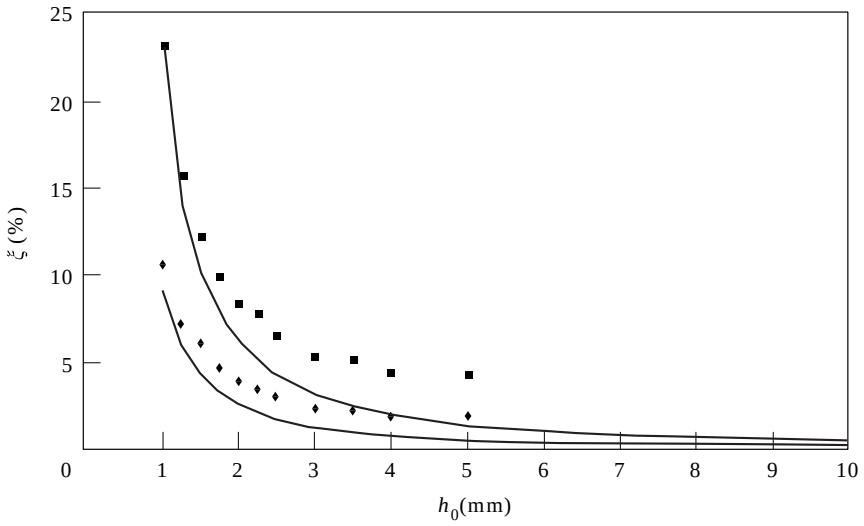

Figure 7. Dimensionless damping coefficient versus gap width: ■, 21; ◆, 11.

calculations and experiments. This indicates that the energy dissipation in the layer is correctly described with the new finite element model.

6.3.3. *Mode shapes*

The mode shapes were calculated and measured for a number of gap widths. In Figure 8 the calculated mode shapes are depicted for gap widths of 300, 50 and 10 mm. The labels of the modes in this figure are based on the corresponding mode shapes in vacuum.

The mode shapes are almost real: the phase differences between the points are very small. The figures indicate that the shape of the asymmetric modes is not affected by the gap width. The symmetric modes however show a dramatic change in shape. For small gaps, the 11-mode starts to resemble the 31-mode. A physical interpretation for these phenomena will be given in the next section.

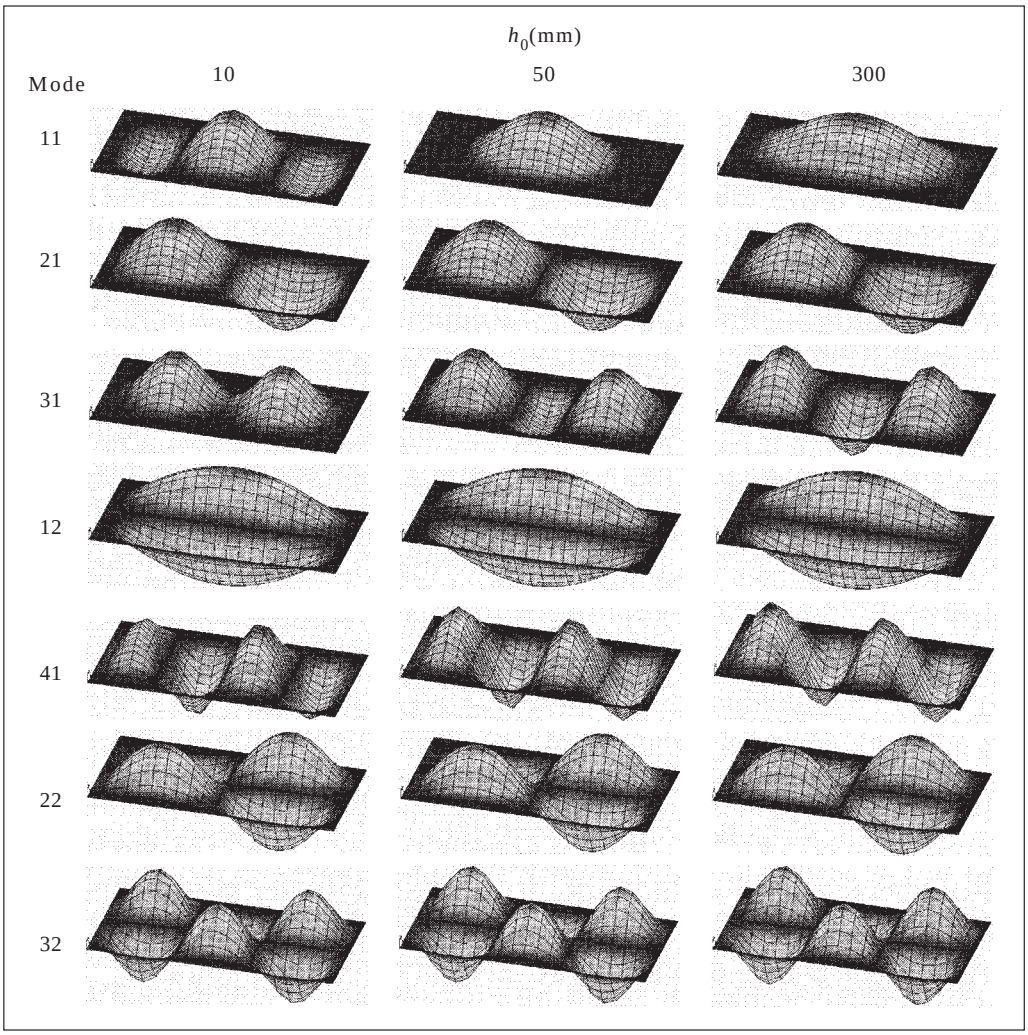

Figure 8. Mode shapes as a function of gap width.

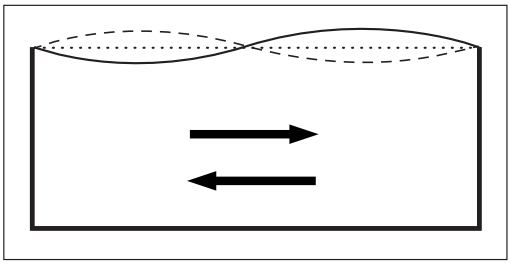

Figure 9. Pumping effect of second mode.

7. PHYSICAL INTERPRETATION

The shifts in eigenfrequency and the changes in mode shape can be explained in terms of (generalized) added mass and (generalized) added stiffness. In section 7.3 an analysis of the dimensionless parameters is given. In Appendix C a very simple mechanical system will be presented which incorporates cross-over effects and changes in mode shapes.

7.1. ADDED MASS

Due to the squeeze motion of the plate the air is put into motion. This motion of the air is experienced by the plate as an added mass. For the closed cavity, the motion of the air is related to the pumping mechanism. For asymmetric modes, the air is pumped back and forth very efficiently (see Figure 9). This pumping effect increases as the gap width decreases. Therefore, the added mass increases and the frequency decreases with decreasing gap width.

7.2. ADDED STIFFNESS

The increase in frequency that was observed for some modes can be attributed to an added stiffness effect. For the symmetric modes, the deformation of the coverplate is accompanied by a significant change in cavity volume (see Figure 10). This change in volume causes a pressure disturbance in the cavity. In the frequency range of interest, the acoustic wavelength is large compared to the cavity dimensions. Since the pressure disturbance acts in phase with the motion of the plate, the plate experiences an added stiffness effect. As the pressure disturbance increases with decreasing gap width, the eigenfrequency will increase. Asymmetric modes do not induce a change in cavity volume: they do not experience an added stiffness effect. Due to the stiffness effect the shape of the symmetric modes also changes. The general trend is that mode shapes tend to a shape

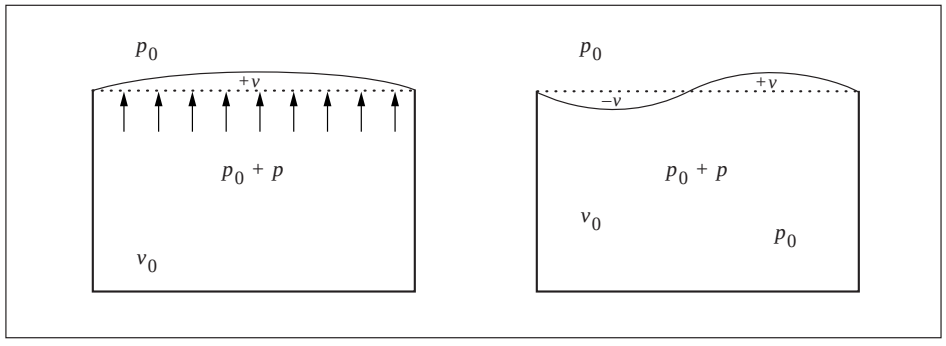

Figure 10. Change in cavity volume for the first and the second mode.

for narrow gaps for which the net volume change is zero (see Figure 8). This means that the added stiffness effect will vanish, and the added mass effect takes over (see Figure 6). This explains the shape of the curves of the eigenfrequencies versus the gap width.

7.3. DIMENSIONLESS PARAMETERS

The parameters are a function of the geometry, the material properties and the frequency. In the experimental set-up the gap width is varied from 50 down to 1 mm, while the frequency varies between 50 and 350 Hz.

7.3.1. *Viscous effects*

The ratio between the inertial forces and the viscous forces is given by the shear wave number. For the experimental set-up, the shear wave number varies from 4·5 to 600. This means that for small gap widths and low frequencies the effects of viscosity have to be taken into account. In the frequency range of interest, the effects of viscosity can be neglected for gap widths larger than 50 mm. The use of standard acoustic elements is therefore justified for these larger gap widths.

7.3.2. *Thermal effects*

For low values of the shear wave number, as σ is a constant for air, the thermal conductivity can play an important role. For the experimental set-up these thermal effects are relatively small. However, one has to be careful not to generalize this statement. For very small gap widths or other materials, for instance, the effects can be very significant. Then the process in the layer has to be regarded as isothermal, rather than isentropic. With the dimensionless parameters one can make a quick estimation for the situation of interest.

7.3.3. *Validity of the narrow gap assumptions*

In the narrow gap theory, two conditions have to hold: $k \ll 1$ and $k/s \ll 1$. In physical terms this means that the acoustic wavelength has to be large compared to both the gap width and the boundary layer thickness. For the experimental set-up both conditions are satisfied: $k \ll 0{\cdot}3$ and $k/s \ll 10^{-3}$. This means that the use of the narrow gap model is justified. If these conditions are not satisfied, one has to resort to the more extensive models, as presented by Kirchhoff, see reference [20] and Bruneau *et al*. [23].

8. CONCLUSIONS

Based on the research presented in this paper, the following conclusions can be drawn.

The viscothermal acoustic finite element gives a good description of the propagation of sound waves in thin layers. It includes the effects of inertia, viscosity, compressibility and thermal conductivity. The element can be used when the acoustic wavelength is large compared to the gap width and the boundary layer thickness.

The acousto-elastic interaction between a thin layer of air and a vibrating flexible surface is correctly described with the finite element model. The behaviour of the system is strongly affected by the presence of the closed layer. It is important to include the acousto-elastic coupling for these situations.

For low shear wave numbers the effects of viscosity have to be taken into account. A significant amount of energy can be dissipated in the layer by means of viscous shear. This may result in substantial damping values for an adjacent structure. The amount of damping is related to the pumping effect in the layer in the low frequency region.

The new finite element model offers an efficient tool for the designer for analyzing complex structures and optimizing the squeeze film damping mechanism.

ACKNOWLEDGMENTS

The authors would like to thank all the people who contributed to this work. The measurements were carried out by Joke Luyten, Stephan Galis and Rob Mathis and were supervised by Bert Wolbert. The authors thank Frank Grooteman and Andre de Boer of the National Aerospace Laboratory for their help and ideas about the implementation in B2000. Finally, the support of the Technology Foundation (STW), Shell and Fokker Space in this research is gratefully acknowledged.

REFERENCES

1. W. M. Beltman, P. J. M. van der Hoogt, R. M. E. J. Spiering and H. Tijdeman 1997 *Journal of Sound and Vibration* **206**, 217–241. Air loads on a rigid plate oscillating normal to a fixed surface.
2. O. Reynolds 1886 *Philosophical Transactions of the Royal Society of London Series A* **177**, 157. On the theory of lubrication.
3. W. Kahlert 1948 *Ingnieur Archiv* **16**, 321–342. Der Einfluß der Trägheitskräfte bei der hydrodynamischen Schmiermittel Theorie (in German).
4. R. S. Brand 1955 *ASME Transactions* **77**, 363–364. Inertia forces in lubricating films.
5. J. V. Beck, W. G. Holliday and G. L. Strodtman 1969 *Journal of Lubrication Technology* **91**, 138–148. Experiment and analysis of a flat disk squeeze-film bearing including effects of supported mass motion.
6. S. M. R. Hashemi and B. J. Roylance 1989 *Tribology Transactions* **32**, 461–468. Analysis of an oscillatory oil squeeze film including effects of fluid inertia.
7. E. C. Kuhn and C. C. Yates 1964 *ASLE Transactions* **7**, 299–303. Fluid inertia effect on the film pressure between axially oscillating parallel circular plates.
8. C. Y. Wang and B. Drachman 1982 *Applied Scientific Research* **39**, 55–68. The steady streaming generated by a vibrating plate parallel to a fixed plate.
9. V. Ramamurthy and U. S. Rao 1987 *Fluid Dynamics Research* **2**, 47–63. The steady streaming generated by a vibrating plate parallel to a fixed plate in a dusty fluid.
10. G. Maidanik 1966 *Journal of the Acoustical Society of America* **40**, 1064–1072. Energy dissipation in associated with gas-pumping in structural joints.
11. E. E. Ungar and J. R. Carbonell 1966 *American Institute of Aeronautics and Astronautics Journal* **4**, 1385–1390. On panel vibration damping due to structural joints.
12. A. D. Pierce 1981 *Acoustics*, *An Introduction to its Physical Principles and Applications*. New York: Acoustical Society of America.
13. M. J. H. Fox and P. N. Whitton 1980 *Journal of Sound and Vibration* **73**, 279–295. The damping of structural vibrations by thin gas films.
14. T. Önsay 1993 *Journal of Sound and Vibration* **163**, 231–259. Effects of layer thickness on the vibration response of a plate–fluid layer system.
15. T. Önsay 1994 *Journal of Sound and Vibration* **178**, 289–313. Dynamic interactions between the bending vibrations of a plate and a fluid layer attenuator.
16. A. Trochidis 1982 *Acustica* **51**, 201–212. Vibration damping due to air or liquid layers.
17. M. Möser 1980 *Acustica* **46**, 210–217. Damping of structure born sound by the viscosity of a layer between two plates.
18. L. C. Chow and R. J. Pinnington 1986 *Journal of Sound and Vibration* **118**, 123–139. Practical industrial method of increasing structural damping in machinery, I: squeeze film damping with air.
19. L. C. Chow and R. J. Pinnington 1988 *Journal of Sound and Vibration* **128**, 333–347. Practical industrial method of increasing structural damping in machinery, I: squeeze film damping with liquids.
20. J. W. S. Rayleigh 1896 *The Theory of Sound* (two volumes, second edition). New York: Dover Publications. See pp. 319–321.
21. M. Bruneau, Ph. Herzog, J. Kergomard and J. D. Polack 1989 *Wave Motion* **11**, 441–451. General formulation of the dispersion equation in bounded visco-thermal fluid, and application to some simple geometries.
22. M. Bruneau, A. M. Bruneau and P. Hamery 1993 *Acta Acustica*, 227–234. An improved approach to modeling the behaviour of thin fluid films trapped between a vibrating membrane and a backing wall and surrounded by a reservoir at the periphery.

23. G. Plantier and M. Bruneau 1990 *Journal d'Acoustique* **3**, 243–250. Heat conduction effects on the acoustic response of a membrane separated by a very thin air film from a backing electrode.
24. C. Karra, M. Ben Tahar, C. Marquette and M. T. Chau 1996 *Proceedings of Internoise* 96, *Liverpool*. (F. Alison Hill and Roy Lawrence, editors), 3003–3006. Boundary element analysis of problems of acoustic propagation in viscothermal fluid.
25. W. M. Beltman, P. J. M. van der Hoogt, R. M. E. J. Spiering and H. Tijdeman 1996 *Proceedings of the International Conference on Spacecraft Structures*, *Materials and Mechanical Testing*, ESA SP-386, *Noordwijk*, *The Netherlands* (W. R. Burke, editor), 219–226. Air loads on solar panels during launch.
26. W. M. Beltman, P. J. M. van der Hoogt, R. M. E. J. Spiering and H. Tijdeman 1996 *Proceedings of ISMA*-21 *Conference on Noise and Vibration Engineering*, *Leuven*, *Belgium* (P. Sas, editor), 1605–1618. Energy dissipation in thin air layers.
27. S. Merazzi 1994 *PhD*. *Thesis* 1251 *EPFL Lausane*, *Switzerland*. Modular finite element analysis tools applied to problems in engineering.
28. M. D. McCollum and C. M. Siders 1996 *Journal of the Acoustical Society of America* **99**, 1949–1957. Modal analysis of a structure in a compressible fluid using a finite element/boundary element approach.
29. E. H. Dowell, G. F. Gorman and D. A. Smith 1977 *Journal of Sound and Vibration* **52**, 519–542. Acousto-elasticity: general theory, acoustic natural modes and forced response to sinusoidal excitation, including comparisons with experiment.
30. R. D. Blevins 1979 *Formulas for Natural Frequency and Mode Shape*. New York: Van Nostrand Reinhold. See p. 418.
31. LMS Numerical Technologies N. V., *SYSNOISE Manual*, Rev. 5.3. Interleuvenlaan 70, 3001 Leuven, Belgium.

APPENDIX A: BASIC EQUATIONS

The basic equations are:

(a) the Navier Stokes equations, for a constant value of the viscosity, μ:

$$\bar{\rho}\left[\frac{\partial \bar{u}}{\partial t}+\bar{u}\frac{\partial \bar{u}}{\partial \bar{x}}+\bar{v}\frac{\partial \bar{u}}{\partial \bar{y}}+\bar{w}\frac{\partial \bar{u}}{\partial \bar{z}}\right]=-\frac{\partial \bar{p}}{\partial \bar{x}}+\mu\left[\frac{\partial^2 \bar{u}}{\partial \bar{x}^2}+\frac{\partial^2 \bar{u}}{\partial \bar{y}^2}+\frac{\partial^2 \bar{u}}{\partial \bar{z}^2}\right]+\frac{1}{3}\mu\frac{\partial}{\partial \bar{x}}\left[\frac{\partial \bar{u}}{\partial \bar{x}}+\frac{\partial \bar{v}}{\partial \bar{y}}+\frac{\partial \bar{w}}{\partial \bar{z}}\right], \tag{A1}$$

$$\bar{\rho}\left[\frac{\partial \bar{v}}{\partial t}+\bar{u}\frac{\partial \bar{v}}{\partial \bar{x}}+\bar{v}\frac{\partial \bar{v}}{\partial \bar{y}}+\bar{w}\frac{\partial \bar{v}}{\partial \bar{z}}\right]=-\frac{\partial \bar{p}}{\partial \bar{y}}+\mu\left[\frac{\partial^2 \bar{v}}{\partial \bar{x}^2}+\frac{\partial^2 \bar{v}}{\partial \bar{y}^2}+\frac{\partial^2 \bar{v}}{\partial \bar{z}^2}\right]+\frac{1}{3}\mu\frac{\partial}{\partial \bar{y}}\left[\frac{\partial \bar{u}}{\partial \bar{x}}+\frac{\partial \bar{v}}{\partial \bar{y}}+\frac{\partial \bar{w}}{\partial \bar{z}}\right], \tag{A2}$$

$$\bar{\rho}\left[\frac{\partial \bar{w}}{\partial t}+\bar{u}\frac{\partial \bar{w}}{\partial \bar{x}}+\bar{v}\frac{\partial \bar{w}}{\partial \bar{y}}+\bar{w}\frac{\partial \bar{w}}{\partial \bar{z}}\right]=-\frac{\partial \bar{p}}{\partial \bar{z}}+\mu\left[\frac{\partial^2 \bar{w}}{\partial \bar{x}^2}+\frac{\partial^2 \bar{w}}{\partial \bar{y}^2}+\frac{\partial^2 \bar{w}}{\partial \bar{z}^2}\right]+\frac{1}{3}\mu\frac{\partial}{\partial \bar{z}}\left[\frac{\partial \bar{u}}{\partial \bar{x}}+\frac{\partial \bar{v}}{\partial \bar{y}}+\frac{\partial \bar{w}}{\partial \bar{z}}\right], \tag{A3}$$

(b) The equation of continuity:

$$\frac{\partial \bar{\rho}}{\partial t}+\frac{\partial(\bar{\rho}\bar{u})}{\partial \bar{x}}+\frac{\partial(\bar{\rho}\bar{v})}{\partial \bar{y}}+\frac{\partial(\bar{\rho}\bar{w})}{\partial \bar{z}}=0; \tag{A4}$$

(c) the equation of state for an ideal gas:

$$\bar{p}=\bar{\rho}R_0\bar{T}, \tag{A5}$$

where R_0 can be written as:

$$R_0=\mathrm{p}_0/\rho_0\mathrm{T}_0; \tag{A6}$$

(d) the energy equation, for a constant value of the thermal conductivity λ and no internal heat generation

$$\rho_0 C_p\left[\frac{\partial \overline{T}}{\partial t}+\bar{u}\frac{\partial \overline{T}}{\partial \bar{x}}+\bar{v}\frac{\partial \overline{T}}{\partial \bar{y}}+\bar{w}\frac{\partial \overline{T}}{\partial \bar{z}}\right]=\lambda\left[\frac{\partial^2 \overline{T}}{\partial \bar{x}^2}+\frac{\partial^2 \overline{T}}{\partial \bar{y}^2}+\frac{\partial^2 \overline{T}}{\partial \bar{z}^2}\right]$$

$$+\frac{\partial \bar{p}}{\partial t}+\bar{u}\frac{\partial \bar{p}}{\partial \bar{x}}+\bar{v}\frac{\partial \bar{p}}{\partial \bar{y}}+\bar{w}\frac{\partial \bar{p}}{\partial \bar{z}}+\mu\Phi, \tag{A7}$$

where Φ is the viscous dissipation function

$$\Phi=2\left[\left(\frac{\partial \bar{u}}{\partial \bar{x}}\right)^2+\left(\frac{\partial \bar{v}}{\partial \bar{y}}\right)^2+\left(\frac{\partial \bar{w}}{\partial \bar{z}}\right)^2\right]-\frac{2}{3}\left[\frac{\partial \bar{u}}{\partial \bar{x}}+\frac{\partial \bar{v}}{\partial \bar{y}}+\frac{\partial \bar{w}}{\partial \bar{z}}\right]^2$$

$$+\left[\frac{\partial \bar{u}}{\partial \bar{y}}+\frac{\partial \bar{v}}{\partial \bar{x}}\right]^2+\left[\frac{\partial \bar{v}}{\partial \bar{z}}+\frac{\partial \bar{w}}{\partial \bar{y}}\right]^2+\left[\frac{\partial \bar{w}}{\partial \bar{x}}+\frac{\partial \bar{u}}{\partial \bar{z}}\right]^2. \tag{A8}$$

Upon assuming sinusoidal motion and no mean flow one can write

$$\begin{aligned}
\bar{u}&=c_0 u(\bar{x},\bar{y},\bar{z})\,e^{i\omega t}, & \bar{p}&=p_0[1+p(\bar{x},\bar{y},\bar{z})\,e^{i\omega t}],\\
\bar{v}&=c_0 v(\bar{x},\bar{y},\bar{z})\,e^{i\omega t}, & \bar{\rho}&=\rho_0[1+\rho(\bar{x},\bar{y},\bar{z})\,e^{i\omega t}],\\
\bar{w}&=c_0 w(\bar{x},\bar{y},\bar{z})\,e^{i\omega t}, & \overline{T}&=T_0[1+T(\bar{x},\bar{y},\bar{z})\,e^{i\omega t}],
\end{aligned} \tag{A9}$$

with u, v, w, p, ρ, and T being small dimensionless perturbations. The mean pressure and the mean density are related according to $p_0=\rho_0 c_0^2/\gamma$.
Dimensionless co-ordinates are introduced:

$$x=\bar{x}/l_x, \qquad y=\bar{y}/l_y, \qquad z=\bar{z}/h_0 \tag{A10}$$

When higher order terms are neglected, the equations can be written in a linearized, dimensionless form. The equations are

$$iu=-\frac{g}{k}\frac{1}{\gamma}\frac{\partial p}{\partial x}+\frac{1}{s^2}\left[g^2\frac{\partial^2 u}{\partial x^2}+\left(\frac{g}{a}\right)^2\frac{\partial^2 u}{\partial y^2}+\frac{\partial^2 u}{\partial z^2}\right]+\frac{1}{3}\frac{g}{s^2}\frac{\partial}{\partial x}\left[g\frac{\partial u}{\partial x}+\left(\frac{g}{a}\right)\frac{\partial v}{\partial y}+\frac{\partial w}{\partial z}\right], \tag{A11}$$

$$iv=-\frac{g}{ak}\frac{1}{\gamma}\frac{\partial p}{\partial y}+\frac{1}{s^2}\left[g^2\frac{\partial^2 v}{\partial x^2}+\left(\frac{g}{a}\right)^2\frac{\partial^2 v}{\partial y^2}+\frac{\partial^2 v}{\partial z^2}\right]+\frac{1}{3}\frac{g}{as^2}\frac{\partial}{\partial y}\left[g\frac{\partial u}{\partial x}+\left(\frac{g}{a}\right)\frac{\partial v}{\partial y}+\frac{\partial w}{\partial z}\right], \tag{A12}$$

$$iw=-\frac{1}{k}\frac{1}{\gamma}\frac{\partial p}{\partial z}+\frac{1}{s^2}\left[g^2\frac{\partial^2 w}{\partial x^2}+\left(\frac{g}{a}\right)^2\frac{\partial^2 w}{\partial y^2}+\frac{\partial^2 w}{\partial z^2}\right]+\frac{1}{3}\frac{1}{s^2}\frac{\partial}{\partial z}\left[g\frac{\partial u}{\partial x}+\left(\frac{g}{a}\right)\frac{\partial v}{\partial y}+\frac{\partial w}{\partial z}\right], \tag{A13}$$

$$g\frac{\partial u}{\partial x}+\left(\frac{g}{a}\right)\frac{\partial v}{\partial y}+\frac{\partial w}{\partial z}=-ik\rho, \tag{A14}$$

$$p=\rho+T, \tag{A15}$$

$$\mathrm{i}T = \frac{1}{s^2\sigma^2}\left[g^2\frac{\partial^2 T}{\partial x^2} + \left(\frac{g}{a}\right)^2\frac{\partial^2 T}{\partial y^2} + \frac{\partial^2 T}{\partial z^2}\right] + \mathrm{i}\left[\frac{\gamma-1}{\gamma}\right]p, \tag{A16}$$

where:

$$s = h_0\sqrt{\frac{\rho_0\omega}{\mu}}, \quad \text{shear wave number,} \quad \sigma = \sqrt{\frac{\mu C_p}{\gamma}}, \quad \text{square root of the Prandtl number,}$$

$$k = \frac{\omega h_0}{c_0}, \quad \text{reduced frequency,} \quad \gamma = \frac{C_p}{C_v}, \quad \text{ratio of specific heats,}$$

$$g = \frac{h_0}{l_x}, \quad \text{narrowness of the gap,} \quad a = \frac{l_y}{l_x}, \quad \text{aspect ratio of the plate.} \tag{A17}$$

When the gap width is small in comparison with the dimensions of the plate, and the velocity w is negligible with respect to the in-plane velocities u and v (i.e., $g \ll 1$, $g/s \ll 1$, $w/v \ll 1$ and $w/u \ll 1$), the equations (A11)–(A16) can be simplified to

$$\mathrm{i}u = -\frac{g}{k}\frac{1}{\gamma}\frac{\partial p}{\partial x} + \frac{1}{s^2}\frac{\partial^2 u}{\partial z^2}, \qquad \mathrm{i}v = -\frac{g}{ak}\frac{1}{\gamma}\frac{\partial p}{\partial y} + \frac{1}{s^2}\frac{\partial^2 v}{\partial z^2}, \qquad 0 = -\frac{1}{k}\frac{1}{\gamma}\frac{\partial p}{\partial z}, \tag{A18–A20}$$

$$g\frac{\partial u}{\partial x} + \left[\frac{g}{a}\right]\frac{\partial v}{\partial y} + \frac{\partial w}{\partial z} = -\mathrm{i}k\rho, \qquad p = \rho + T, \qquad \mathrm{i}T = \frac{1}{s^2\sigma^2}\frac{\partial^2 T}{\partial z^2} + \mathrm{i}\left[\frac{\gamma-1}{\gamma}\right]p. \tag{A21–A23}$$

The boundary conditions are

$$\begin{aligned} &\text{at } z = 0, \quad u = 0, \quad v = 0, \quad w = 0, \quad T = 0 \quad \text{(isothermal wall),} \\ &\text{at } z = 1, \quad u = 0, \quad v = 0, \quad w = \mathrm{i}kh, \quad T = 0 \quad \text{(isothermal wall).} \end{aligned} \tag{A24}$$

From equation (A20) it follows that the magnitude of the pressure perturbation, p, depends only on the in-plane co-ordinates x and y. Because the pressure perturbation is independent of the co-ordinate z, the solution of equation (A23) can be written as

$$T = \left[\frac{\gamma-1}{\gamma}\right]pA(s\sigma, z), \tag{A25}$$

where

$$A(s\sigma, z) = \left[\frac{\sinh\left(s\sigma\sqrt{\mathrm{i}}(z-1)\right) - \sinh\left(s\sigma\sqrt{\mathrm{i}}z\right)}{\sinh\left(s\sigma\sqrt{\mathrm{i}}\right)} + 1\right]. \tag{A26}$$

Substitution of equation (A25) into equation (A22) gives

$$\rho = p\left\{1 - \left[\frac{\gamma-1}{\gamma}\right]A(s\sigma, z)\right\}. \tag{A27}$$

The solution of equation (A18) can be written in the following form:

$$u = \mathrm{i}\frac{g}{k}\frac{1}{\gamma}\left(\frac{\partial p}{\partial x}\right)A(s, z). \tag{A28}$$

Similarly, it follows that:

$$v = \mathrm{i}\,\frac{g}{ak}\,\frac{1}{\gamma}\left(\frac{\partial p}{\partial y}\right) A(s, z). \tag{A29}$$

Finally, the equation of continuity (A21) has to be satisfied. Inserting the equations (A28), (A29) and (A27) gives

$$\mathrm{i}\,\frac{g^2}{k}\,\frac{1}{\gamma}\left(\frac{\partial^2 p}{\partial x^2}\right) A(s, z) + \mathrm{i}\,\frac{g^2}{a^2 k}\,\frac{1}{\gamma}\left(\frac{\partial^2 p}{\partial y^2}\right) A(s, z) + \frac{\partial w}{\partial z} = -\mathrm{i}kp\left\{1 - \left[\frac{\gamma - 1}{\gamma}\right] A(s\sigma, z)\right\}. \tag{A30}$$

Integrating with respect to z gives:

$$\mathrm{i}\,\frac{g^2}{k}\,\frac{1}{\gamma}\left(\frac{\partial^2 p}{\partial x^2}\right) B(s) + \mathrm{i}\,\frac{g_y^2}{a^2 k}\,\frac{1}{\gamma}\left(\frac{\partial^2 p}{\partial y^2}\right) B(s) + w_1 - w_0 = -\mathrm{i}kp\left\{1 - \left[\frac{\gamma - 1}{\gamma}\right] B(s\sigma)\right\}, \tag{A31}$$

where

$$B(s) \equiv \int_{z=0}^{1} A(s, z)\,\mathrm{d}z = 2\left[\frac{1 - \cosh\,(s\sqrt{\mathrm{i}})}{s\sqrt{\mathrm{i}}\,\sinh\,(s\sqrt{\mathrm{i}})}\right] + 1. \tag{A32}$$

Rearranging equation (A31) for the pressure perturbation p yields

$$g^2\left(\frac{\partial^2 p}{\partial x^2}\right) + \left(\frac{g}{a}\right)^2\left(\frac{\partial^2 p}{\partial y^2}\right) = \frac{k\gamma}{B(s)}\left[-kp\left\{1 - \left[\frac{\gamma - 1}{\gamma}\right] B(s\sigma)\right\} + \mathrm{i}\{w_1 - w_0\}\right]. \tag{A33}$$

The dimensionless velocities w_1 and w_0 can be expressed as in equation (A24). Substitution of equation (A24) into equation (A33) finally gives the equation for the pressure perturbation p in the gap:

$$g^2\left(\frac{\partial^2 p}{\partial x^2}\right) + \left(\frac{g}{a}\right)^2\left(\frac{\partial^2 p}{\partial y^2}\right) = -\frac{k^2\gamma}{B(s)}\left[p\left\{1 - \left[\frac{\gamma - 1}{\gamma}\right] B(s\sigma)\right\} + h\right]. \tag{A34}$$

From equation (A34) the expression for the (complex) polytropic constant n can be obtained (note that this constant was obtained by integrating over the layer thickness):

$$n(s\sigma) = \left[1 - \left[\frac{\gamma - 1}{\gamma}\right] B(s\sigma)\right]^{-1}. \tag{A35}$$

Substitution of equation (A35) into equation (A34) finally gives the "narrow gap" equation:

$$g^2\left(\frac{\partial^2 p}{\partial x^2}\right) + \left(\frac{g}{a}\right)^2\left(\frac{\partial^2 p}{\partial y^2}\right) = -\frac{k^2\gamma}{B(s)}\left[\frac{p}{n(s\sigma)} + h\right]. \tag{A36}$$

APPENDIX B: FINITE ELEMENT MODEL

As a starting point, the differential equation (12) is multiplied by a weighting function w^w and integrated over the area Γ:

$$\int_\Gamma w^w \left[\nabla^2 \bar{p} + \frac{\omega^2}{c_{eff}^2(s)} \bar{p} \right] \mathrm{d}\Gamma = -\frac{\rho_0 \omega^2}{h_0 B(s)} \int_\Gamma w^w \mathbf{n} \cdot \bar{\mathbf{u}}^s \, \mathrm{d}\Gamma \tag{B1}$$

where $\bar{\mathbf{u}}^s$ is the structural displacement and $\mathbf{n}$ is the outward normal. Note that $\mathbf{n} \cdot \bar{\mathbf{u}}^s = \bar{h} - h_0$. Using partial integration and Green's theorem one has

$$\int_{\partial\Gamma} w^w \frac{\partial \bar{p}}{\partial n} \, \mathrm{d}\partial\Gamma - \int_\Gamma \nabla w^w \cdot \nabla \bar{p} \, \mathrm{d}\Gamma + \frac{\omega^2}{c_{eff}^2(s)} \int_\Gamma w^w \bar{p} \, \mathrm{d}\Gamma = -\frac{\rho_0 \omega^2}{h_0 B(s)} \int_\Gamma w^w \mathbf{n} \cdot \bar{\mathbf{u}}^s \, \mathrm{d}\Gamma, \tag{B2}$$

where $\partial\Gamma$ is the boundary of the domain Γ. The pressure in each element is expressed in terms of the interpolation functions $[N^a]$ and the nodal pressure $\{\mathbf{P}\}$. The structural displacement is also written in terms of interpolation functions:

$$\bar{p}(\mathbf{x}) = [N^a(\mathbf{x})]\{\mathbf{P}\}, \qquad \bar{\mathbf{u}}^s(\mathbf{x}) = [N^s(\mathbf{x})]\{\mathbf{U}\}. \tag{B3}$$

Following Galerkin's approach, the weighting functions are chosen equal to the interpolation functions. For a rigid wall, the normal derivative of the pressure is zero. In case of a prescribed pressure the weighting function is chosen equal to zero. The first term of equation (B2) only contributes for an impedance-like boundary condition. However, one has to bear in mind that the pressure is constant across the gap width, while the in-plane velocities vary.

Defining an impedance can therefore only be done in an integrated sense. This term is set equal to zero in the present study. This finally leads to the sets of equations

$$-\omega^2 [M^a(s)]\{\mathbf{P}\} + [K^a]\{\mathbf{P}\} = \omega^2 [M^c(s)]\{\mathbf{U}\}, \tag{B4}$$

where $[M^a(s)]$ denotes the acoustic mass matrix, $[K^a]$ is the acoustic stiffness matrix, $\{\mathbf{P}\}$ is the vector with the nodal pressure degrees of freedom, $\{\mathbf{U}\}$ is the vector with the nodal structural degrees of freedom and $[M^c(s)]$ is the coupling matrix. Their elements are given by

$$[M^a(s)] = \frac{1}{c_{eff}^2(s)} \int_\Gamma [N^a]^{\mathrm{T}} [N^a] \, \mathrm{d}\Gamma, \qquad [K^a] = \int_\Gamma [\nabla N^a]^{\mathrm{T}} \cdot [\nabla N^a] \, \mathrm{d}\Gamma,$$

$$[M^c(s)] = \frac{\rho_0}{h_0 B(s)} \int_\Gamma [N^a]^{\mathrm{T}} [\mathbf{n} \cdot N^s] \, \mathrm{d}\Gamma. \tag{B5–B7}$$

The finite element model for the structure, in the absence of structural damping, can be written in the standard formulation as

$$-\omega^2 [M^s]\{\mathbf{U}\} + [K^s]\{\mathbf{U}\} = [K^c]\{\mathbf{P}\} + \{\mathbf{F}^{ext}\}, \tag{B8}$$

where $[M^s]$ denotes the structural mass matrix, $[K^s]$ is the stiffness matrix, $[K^c]$ is the coupling matrix resulting from the pressure on the interface and $\{\mathbf{F}^{ext}\}$ is the external nodal force vector. Using the same interpolation for the pressure in the layer and the pressure

excitation on the structure, the principle of virtual work gives the following expression for the coupling matrix $[K^c]$:

$$[K^c] = \int_\Gamma [\mathbf{n} \cdot N^s]^T [N^a] \, d\Gamma. \tag{B9}$$

The acousto-elastic interaction is established by demanding continuity of normal velocity across the interface. This now gives the following coupled system of equations:

$$-\omega^2 \begin{bmatrix} [M^s] & [0] \\ [M^c(s)] & [M^a(s)] \end{bmatrix} \begin{Bmatrix} \{\mathbf{U}\} \\ \{\mathbf{P}\} \end{Bmatrix} + \begin{bmatrix} [K^s] & -[K^c] \\ [0] & [K^a] \end{bmatrix} \begin{Bmatrix} \{\mathbf{U}\} \\ \{\mathbf{P}\} \end{Bmatrix} = \begin{Bmatrix} \{\mathbf{F}^{ext}\} \\ \{\mathbf{0}\} \end{Bmatrix}. \tag{B10}$$

This system contains the mass matrices and the stiffness matrices of the structural part and the acoustic part. The coupling is established by the two coupling matrices, $[M^c(s)]$ and $[K^c]$, which are related by

$$[M(s)^c] = \frac{\rho_0}{h_0 B(s)} [K^c]^T. \tag{B11}$$

APPENDIX C: CROSS-OVER BEHAVIOUR

In Figure C1 a simple beam model is given which is used to illustrate the cross-over phenomenon. The beam's properties are

$$E_p = 210 \times 10^9 \text{ N/m}^2, \qquad t_p = 1 \times 10^{-3} \text{ m}, \qquad l_x = 0{\cdot}245 \text{ m}, \qquad \rho_p = 2710 \text{ kg/m}^3. \tag{C1}$$

A beam with length $2l_x$ and thickness t_p is simply supported. It is located in vacuum and is supported by a spring in the centre. The spring represents the added stiffness effects of the air layer. Since the spring is located in the centre, the eigenfrequencies of asymmetric modes will not be affected by the stiffness of the spring. The eigenfrequencies of the symmetric modes, however, will be affected, in accordance with the explanation given in section 7.2. The stiffness of the spring depends on the value of a parameter, h_0, which of course represents the gap width. The stiffness of the spring increases with decreasing gap width. The following expression was used in this example for the stiffness k_v:

$$k_v(h_0) = 2 \times 10^4 \left[\frac{1 - h_0}{h_0} \right]^2. \tag{C2}$$

The eigenfrequencies and the mode shapes of the plate were calculated as a function of h_0. The displacement was written in terms of the mode shapes of a simply supported beam. The participation factors were calculated with a Rayleigh Ritz procedure. This approach allows one to decompose the mode shape in terms of the mode shapes in vacuum, i.e.,

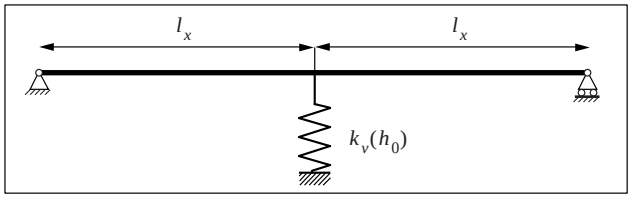

Figure C1. Simple mechanical model.

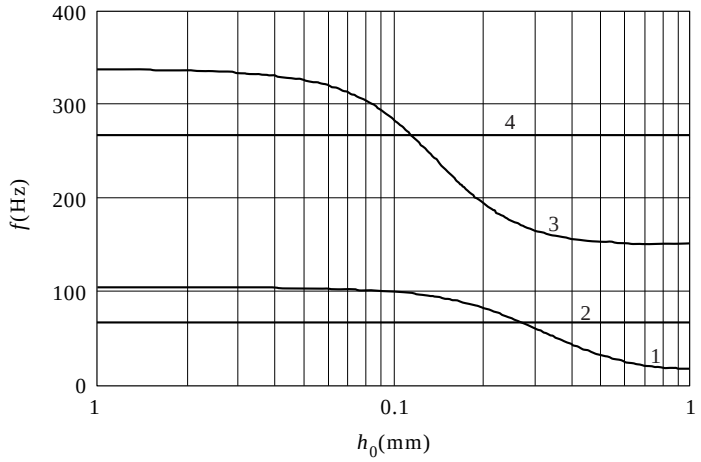

Figure C2. Eigenfrequency versus gap width for beam model.

without the spring. The eigenfrequency as a function of h_0 is given in Figure C2. The figure shows the same cross-over behaviour as the results for the airtight box. Asymmetric modes are not affected by the gap width in this example, since there is no added mass effect. The symmetric modes, however, are affected by the added stiffness effect, which results in an increase in frequency. Due to this phenomenon several cross-overs are present. This simple example illustrates that crossing of frequencies is not unusual for mechanical systems.

In section 6 it was observed that for instance the first mode of the plate starts to resemble the third mode in vacuum for small gaps. The same trend can be recognized in the results for the beam model. The participation factor for large gap widths is almost 1 for the 11-mode. As the gap width decreases, the participation factors for other contributions increase. The 31-mode exhibits similar behaviour. It can be concluded that this simple mechanical model incorporates many characteristics of the acousto-elastic system.

APPENDIX D: LIST OF SYMBOLS

A	function describing velocity and temperature profiles
B	function accounting for viscous or thermal effects
$a = l_y/l_x$	aspect ratio
C_p	specific heat at constant pressure
C_v	specific heat at constant volume
c_0	undisturbed speed of sound
c_{eff}	effective speed of sound
D_p	bending stiffness of plate
E_p	Young's modulus of plate material
f	frequency
$g = h_0/l_x$	dimensionless gap width
$\overline{h} = h_0[1 + h\ \mathrm{e}^{\mathrm{i}\omega t}]$	gap width
h_0	mean gap width
h	dimensionless displacement amplitude
$\mathrm{i} = \sqrt{-1}$	imaginary unit
$k = \omega h_0/c_0$	reduced frequency
k_v	spring stiffness
l_x	length in the x direction
l_y	length in the y direction
n	polytropic constant
$\mathbf{n}$	normal vector

$\tilde{p} = p_0[1 + p\ \mathrm{e}^{\mathrm{i}\omega t}]$	pressure
p_0	mean pressure
p	dimensionless pressure amplitude
R_0	gas constant
$s = h_0\sqrt{\rho_0\omega/\mu}$	shear wave number
$\tilde{T} = T_0[1 + T\mathrm{e}^{\mathrm{i}\omega t}]$	temperature
T_0	mean temperature
T	dimensionless temperature amplitude
t	time
t_p	plate thickness
$\tilde{u} = c_0 u\ \mathrm{e}^{\mathrm{i}\omega t}$	velocity in the x direction
u	dimensionless amplitude of the velocity in the x direction
$\tilde{\mathbf{u}}^s$	structural displacement vector
$\tilde{v} = c_0 v\ \mathrm{e}^{\mathrm{i}\omega t}$	velocity in the y direction
v	dimensionless amplitude of the velocity in the y direction
$\tilde{w} = c_0 w\ \mathrm{e}^{\mathrm{i}\omega t}$	velocity in the z direction
w	dimensionless amplitude of the velocity in the z direction
w^w	weighting function
$\tilde{x} = l_x x$	x co-ordinate
x	dimensionless x co-ordinate
$\mathbf{x}$	spatial co-ordinates (vector)
$\tilde{y} = l_y y$	y co-ordinate
y	dimensionless y co-ordinate
$z = h_0 z$	z co-ordinate
z	dimensionless z co-ordinate
Γ	integration domain
$\partial\Gamma$	boundary of integration domain
$\gamma = C_p/C_v$	ratio of specific heats
$\varepsilon = \rho_0 h_0/\rho_p t_p$	ratio of mass per unit area
λ	thermal conductivity of air
μ	dynamic viscosity of air
ξ	dimensionless damping coefficient
ν_p	Poisson's ratio of plate material
$\tilde{\rho} = \rho_0[1 + \rho\ \mathrm{e}^{\mathrm{i}\omega t}]$	density of air
ρ_0	mean density of air
ρ	dimensionless density amplitude
ρ_p	density of plate material
$\sigma = \sqrt{\mu C_p/\lambda}$	square root of the Prandtl number
Φ	viscous dissipation function
Ω	dimensionless frequency
ω	angular frequency
∇	gradient operator
$\{\mathbf{F}^{ext}\}$	structural external force vector
$[K^a]$	acoustic stiffness matrix
$[K^c]$	coupling stiffness matrix
$[K^s]$	structural stiffness matrix
$[M^a(s)]$	acoustic mass matrix
$[M^c(s)]$	coupling mass matrix
$[M^s]$	structural mass matrix
$[N^a]$	acoustic interpolation functions
$[N^S]$	structural interpolation functions
$\{\mathbf{P}\}$	acoustic pressure degrees of freedom
$\{\mathbf{U}\}$	structural degrees of freedom